Nanoscale corrosion behavior of polycrystalline copper fine wires in dilute NaCl solution investigated by in-situ atomic force microscopy

doi: 10.1016/j.corsci.2016.01.015

Nanoscale corrosion behavior of polycrystalline copper fine wires in dilute NaCl solution investigated by *in-situ* atomic force microscopy

Shoichiro Ogata[a,1], Naritaka Kobayashi[a,2], Takuya Kitagawa[a], Shohei Shima[b], Akira Fukunaga[b], Chikako Takatoh[b], Takeshi Fukuma[a,*]

[a] *Division of Electrical Engineering and Computer Science, Kanazawa University, Kanazawa 920-1192, Japan*
[b] *EBARA Corporation, Tokyo 144-8510, Japan*

Abstract

In this study, nanoscale corrosion behavior of copper fine wires in dilute NaCl solution is studied by atomic force microscopy and electron backscatter diffraction technique. The dissolution rate of the grains constituting the wires strongly depends on their crystallographic orientation. In pure water, the dissolution rate increases in the order of (111) < (001) < (110). Addition of Cl^- dramatically increases the dissolution rate of the (111) surface to alter the order to (110) ≈ (001) ≈ (111) at 0.1 mM. These results show that the crystallographic orientation dependence is significantly changed by a slight increase of Cl^- concentration in dilute solution.

Keywords: A. Copper, B. AFM, C. Anodic dissolution

1. Introduction

Corrosion of copper fine wires during fabrication of semiconducting devices has been a serious problem. To fabricate copper fine wires, a patterned trench structure on a Si wafer is formed by photolithography and a copper thin film is

*Corresponding author
Email address: fukuma@staff.kanazawa-u.ac.jp (Takeshi Fukuma)
[1]Present address: EBARA Corporation, Tokyo 144-8510, Japan
[2]Present address: Division of Strategic Research and Development, Saitama University, Saitama 338-8570, Japan

deposited on it. Subsequently, the surface is flattened by chemical mechanical polishing (CMP), where a rotating wafer is pressed against a fixed polishing pad in a slurry solution. The solution contains anticorrosive molecules to form a protective layer on the copper surface. Thus, the polished copper surface is protected during the polishing and subsequent transfer of the wafer to the next process. However, before proceeding to the next process, the protective layer should be removed by gently scrubbing the surface in a cleaning solution. Although the solution contains another anticorrosive component, it is gradually replaced with pure water before drying. During this cleaning process, a copper surface is exposed to a dilute ionic solution and partially dissolves to form defects: locally etched spots showing high electrical resistance in a wire. To prevent such corrosion, it is essential to understand nanoscale corrosion processes of a copper fine wire in a dilute ionic solution.

So far, corrosion behavior of various metals in different solutions has been investigated. Among them, copper corrosion in pure water[1–4] and Cl^- solution[5–10] is one of the most extensively studied examples. This is due to the wide use of copper materials and the ubiquity of Cl^- in an aqueous environment (e.g. sea water and tap water). Macroscopic corrosion behavior is mainly studied by electrochemical measurement techniques while microscopic behavior is analyzed by optical, electron or x-ray beam technologies as well as scanning probe microscopy (SPM)[6–10]. However, microscopic studies on copper fine wires are limited[11]. In addition, previous studies were mainly performed at a high Cl^- concentration[5–10] due to the strong interests in the corrosion caused by sea water. Therefore, microscopic corrosion behavior of copper fine wires in a dilute Cl^- solution has not been well understood in spite of its importance in semiconductor industry.

Recently, SPM techniques such as scanning tunneling microscopy (STM)[12], atomic force microscopy (AFM)[13] and scanning electrochemical microscopy (SECM)[14] have been proven to be a powerful tool for studying microscopic corrosion processes. As they can be operated in liquid, *in-situ* measurements of microscopic corrosion behavior can be performed. Furthermore, when it

is used with electron backscatter diffraction (EBSD) measurement technique, crystallographic orientation dependence of corrosion behavior can be studied[6–10]. According to these previous studies, microscopic metal corrosion behavior strongly depends on crystallographic orientation. In addition, Lapeire et al. reported that the crystallographic orientation of the neighboring grains can also influence the corrosion behavior[7]. Copper fine wires consist of plated polycrystalline thin film having nanoscale domains with different crystallographic orientations. Therefore, to understand their corrosion behavior, it is essential to use a microscopic technique having a nanoscale spatial resolution in liquid.

In this study, nanoscale corrosion processes of copper fine wires in dilute NaCl solution is studied by *in-situ* AFM and *ex-situ* EBSD measurements. AFM measurements in different NaCl concentration were performed. Comparing the AFM images with inverse pole figure (IPF) maps obtained by EBSD, dependence of the nanoscale corrosion behavior on crystallographic orientation and NaCl concentration is clarified. A possible model to explain the observed corrosion behavior is also presented.

2. Material and methods

2.1. Copper fine wires

For the AFM and EBSD measurements, patterned copper fine wires fabricated on a Si wafer (854 Cu CMPd Wafer, Advanced Materials Technology) was used. Figure 1(a) shows a large-scale view of the pattern while Figure 1(b) shows a magnified view of the area that was measured by AFM and EBSD. In this region, the line and space width is 1 μm. The two wires at the center are connected to a 0.1 mm $\times$ 0.1 mm copper pad while the others are electrically isolated. Owing to the characteristic wiring pattern in this area, its location can be easily identified either by scanning electron microscopy (SEM) or optical microscopy. This enables to analyze the same area by AFM and EBSD.

Figure 1(c) shows a cross section of one of the wires shown in Fig. 1(b). As illustrated in this cross section, the copper wires are formed on a 25 nm Ta film

and have a depth of 475 nm. The outline of the fabrication process is as follows.

1. A patterned trench structures were formed by etching the SiO_2 layer.
2. A 25 nm Ta film was formed on the wafer surface by physical vapor deposition (PVD).
3. A thick copper film was formed on the Ta film by electroplating.
4. The wafer was annealed at 150°C for 30 min.
5. The surface was polished by CMP to make the SiO_2 thickness 500 nm, which corresponds to the copper wire thickness of 475 nm.

In this way, polycrystalline copper fine wires were fabricated. The wires consist of nanoscale grains with different crystallographic orientations. For the AFM and EBSD measurements, the wafer was cut into 10 mm × 10 mm pieces such that each sample should have the same type of copper wire pattern at its center.

2.2. AFM and EBSD measurements

In this study, AFM measurements were performed in pure water and 0.01 mM/0.1 mM NaCl solution. For each experiment, a different piece of sample was used. Before the AFM measurements, an EBSD measurement was performed to obtain an IPF map of the copper wires. For the measurements, field-emission scanning electron microscopy (JIB-4601F, JEOL) and EBSD detector and software (TSL Solutions) were used. The acceleration voltage and current of the electron beam were 20 kV and 1 nA, respectively.

During the EBSD measurements, carbon contaminations were deposited on the surface. To remove such contaminations, the surface was cleaned by Ar plasma cleaner (SC-701, Sanyu Electronics). The Ar plasma cleaning with a typical operating condition can severely damage the copper wires. Thus, the bias voltage and the inlet gas pressure were adjusted to just as high as required for maintaining the plasma. In addition, the sample was covered with a Cu plate to suppress the electric field applied to the sample surface. Under this condition, the damage of the wires caused by the cleaning is negligible.

After the Ar plasma cleaning, the sample was attached onto a sample holder for the AFM used in this experiment. On the fixed sample, a 100 μL 0.5

M citric acid solution was dropped and left it for 1 min to remove organic contaminations deposited on the surface during the sample transfer process. Subsequently, the deposited solution was replaced with pure water by gentle pipetting. This process was repeated for five times not only to completely replace the solution but also to rinse the surface with pure water. Although the copper surface partially dissolves in the citric acid, the created height variations do not significantly influence following discussions, where time-dependent height changes of the copper wires are compared between different solution conditions and crystallographic orientations.

The sample holder was set onto the AFM system. Just before starting the tip coarse approach process, the water on the sample was replaced with an imaging solution, which is either pure water, 0.01 mM or 0.1 mM NaCl solution. Note that the term 'imaging solution' is used to refer to 'solution in which AFM imaging was performed'. This process was repeated twice to completely replace the solution with the imaging solution. The elapsed time was recorded since this replacement as each AFM image was saved.

In this experimental procedure, it is very important to keep the sample surface wet after the cleaning by citric acid. Experiments without a cleaning by citric acid or with an exposure of the surface to the air after the cleaning results in poor reproducibility due to the contaminations deposited on the copper surface during the exposure to the air. This is particularly evident for an experiment in dilute NaCl solution, where relatively minor corrosion processes must be accurately analyzed.

AFM measurements were performed by a custom-built amplitude-modulation AFM (AM-AFM)[15–17] in the imaging solution. AFM images were obtained in the constant amplitude mode, where the tip-sample distance is controlled such that cantilever oscillation amplitude is kept constant. A commercially available AFM controller (RC4/OC4, SPECS) was used for the AFM operation. Si cantilevers (AC55, Olympus) having a spring constant of $\sim$80 N/m, a resonance frequency (f_0) of $\sim$1.3 MHz and Q factor of $\sim$12 in aqueous solution were used.

3. Results

Corrosion process of copper wires in water was imaged by AFM from 39 min till 203 min since the surface was immersed in the imaging solution. Figures 2(a, b) show AFM images of copper wires in water at 39 min and 203 min, respectively. See also a video consisting of all the AFM images obtained during the corrosion process (Water.gif in supplementary online materials). The images show four copper wires as illustrated in Fig. 1(b). At 39 min, the copper surface already shows nanoscale height variations. Such initial height variations may be caused by the CMP, Ar plasma or citric acid cleaning. As the main interest of this work is on the copper corrosion processes in dilute NaCl solution, hereafter we do not discuss formation mechanism of these initial height variations but focus on the time-dependent height changes observed during the AFM imaging. The image obtained at 203 min shows a larger local height variation than the one obtained at 39 min. This result shows that the corrosion resistance is not uniform but has local variation.

Figure 2(c) shows an IPF map of the same area as imaged by AFM. Comparison between the IPF and AFM images reveals that the local areas showing different corrosion resistance approximately correspond to the grains with different crystallographic orientations. The result shows that the corrosion resistance is strongly dependent on the crystallographic orientation.

Table 1: Dissolution rates (unit: pm/min) measured in different solution at positions 1-3 indicated in Figs. 2-4 Avg and SD denote average and standard deviation of the values measured at positions 1-3.

	Water			0.01 mM			0.1 mM		
	(110)	(001)	(111)	(110)	(001)	(111)	(110)	(001)	(111)
1	20.6	5.4	1.7	16.3	32.1	19.5	21.2	23.8	40.4
2	22.2	5.1	0.6	21.9	33.1	21.9	26.8	20.2	33.2
3	25.5	6.0	2.3	26.5	26.5	31.1	—	21.0	25.6
Avg	22.8	5.5	1.5	21.6	30.6	24.2	24.0	21.7	33.1
SD	2.5	0.5	0.9	5.1	3.6	6.1	4.0	1.9	7.4

To investigate the correlation between the crystallographic orientation and the corrosion resistance, height changes at three locations were analyzed for each of the (110), (001) and (111) surfaces as indicated by the arrows. Note that all the locations were selected from the same wire to eliminate possible influence of the difference in the macroscopic wiring pattern. Fig. 2(d) shows the height changes at the locations indicated by the arrows No. 1 in Fig. 2(c). The curves show that the height decreases almost linearly at these locations. Thus, we calculated the average dissolution rates at positions 1-3 from the initial and final surface heights as summarized in Table 1.

Similar analyses of the copper corrosion were performed in 0.01 mM and 0.1 mM NaCl solution as shown in Figures 3 and 4. See also videos consisting of all the AFM images obtained during the corrosion processes (001mM.gif and 01mM.gif in supplementary online materials). AFM images shown in Figure 4 may appear to have a low resolution compared to the other images. This is not due to the pixel resolution but the contaminations on the tip apex. As Cl^- concentration increases, the dissolution rate increases, making it difficult to keep the tip apex clean. However, this does not significantly influence the accuracy of the height measurements. The average dissolution rates measured at all the locations in different solution are summarized in Table 1 and Figure 5.

Due to the limited number of the grains in one wire and hence the data points, the obtained data has a relatively large error bars (i.e. standard deviation). To evaluate the significance of the difference in the mean values between the data sets, two-tailed T-tests were performed with a significance level of $\alpha = 0.05$. Following discussions are made based on these statistical analyses.

In pure water, the dissolution rate increases in the order of (111), (001) and (111). However, the addition of Cl^- into water significantly increases the dissolution rate of the (001) and (111) surfaces while it gives little influence on the dissolution rate of the (110) surface. Further increase of Cl^- concentration from 0.01 mM to 0.1 mM decreases the dissolution rate of the (001) surface. Although the mean value of the dissolution rate of the (001) surface increases,

the significance of the difference is not confirmed due to the large error bars. For 0.01 mM and 0.1 mM NaCl solution, the dissolution rate shows no significant difference between different crystallographic orientations.

4. Discussion

From the results presented above, at least two major findings are obtained.

1. The dissolution rate in pure water increases in the order of the (111), (001) and (110) surfaces.
2. The dissolution rate of the (111) surface dramatically increases with increasing the Cl^- concentration.

Two sets of similar experiments were performed and reproducibility of these two major findings were confirmed. Here, the mechanism underlying these corrosion behaviors is discussed.

4.1. Corrosion in pure water

In pure water, copper corrosion is caused by the following reaction.

$$Cu \rightleftharpoons Cu^{2+} + 2e^- \tag{1}$$

However, a copper surface should be covered with an oxide layer in an aqueous environment. Note that the surface oxide layer was once removed by the citric acid cleaning. However, we replaced the citric acid with pure water and subsequently with an imaging solution. Thus, by the time we started the imaging, the surface had been immersed in aqueous solution for several tens of minutes and hence covered with an oxide layer formed after the citric acid cleaning.

The copper oxidation and its influence on corrosion resistance have been investigated by various methods[18–29]. Most of these studies reported that the initial oxide layer mainly consists of Cu_2O rather than CuO or $Cu(OH)_2$[20, 22, 24–27]. The Cu_2O layer serves as a protective layer against corrosion. Thus, the observed difference in the dissolution rate should represent the difference in the corrosion resistance of the Cu_2O layer.

There have been several studies on crystallographic orientation dependence of copper oxide films formed by anodic oxidation[8, 26, 30–34]. Previous AFM and STM studies[30–32, 34] showed that a Cu_2O(111) film is epitaxially grown on Cu(111) while a Cu_2O(001) film is epitaxially grown on Cu(001) in 0.1 M NaOH solution. Kunze et al. reported that the Cu_2O film formed on Cu(111) by anodic oxidation is thicker than that on Cu(001)[34]. Gao et al. reported that an oxide film formed on Cu(111) by thermal annealing is thicker than that on Cu(110) and Cu(001)[26]. Martinez-Lombardia et al. reported that the passive layer formed by anodic oxidation on Cu(111) has a lower conductivity or reactivity than that on Cu(001)[8]. They tentatively explained the observed difference by the difference in the defect density. Although the oxide films formed in these previous studies are not prepared by the same procedure or in the same environment, they consistently show a similar dependence on the crystallographic orientation. Namely, a Cu_2O layer formed on Cu(111) has a higher thickness and corrosion resistance than that on Cu(001).

The corrosion resistance increases in the order of (110), (001) and (111) in pure water. This result is consistent with the previous reports described above. The same order is found for different physical quantities. The surface energy decreases[35], the work function increases[36], the atomic density increases, and the surface corrugation decreases in the order of (110), (001) and (111). These results suggest that the (111) surface should show the highest crystalinity and the lowest defect density. As a Cu_2O film is epitaxially grown on Cu(111), this should be also true of the oxide layers formed on a copper surface. Therefore, the observed difference in the corrosion resistance probably originates from the difference in the defect density of the oxide layer. This interpretation is consistent with previous reports on the corrosion mechanism of an oxidized copper surface. According to the previous review by Kear et al., the copper dissolution takes place due to the charge and material transports through the defects in the Cu_2O layer and the corrosion products made of $CuO/Cu(OH)_2$ are deposited on the oxidized surface[5].

Lapeire et al. previously investigated crystallographic orientation depen-

dence of copper corrosion in 0.1 M NaCl and 0.5 M Na_2SO_4 by AFM and EBSD[7]. They found that the (111) surface dissolves faster than the (001) surface when they are adjacent to each other. In this study, the (111) grains indicated by arrows 1-3 are all adjacent to the (001) grains as shown in Fig. 2(c). However, they consistently showed a lower dissolution rate than that of the (001) grains (Fig. 5 and Table 1). This disagreement suggests that such influence of neighboring grains in pure water may be weaker than that in 0.1 M NaCl solution.

4.2. Corrosion in dilute Cl^- solution

In pure water, the dissolution rate of the (111) surface is lower than that of the (110) and (001) surfaces. However, it is dramatically increased by adding Cl^-. At 0.1 mM, the dissolution rate of the (111) surface becomes as high as that of the other surfaces. According to previous studies, the dissolution rate of the (111) surface becomes higher than that of the (001) surface at a higher Cl^- concentration. Martinez-Lombardia et al. investigated the reactivity of the (111) and (001) surfaces in an active state in 5 mM NaCl solution by SECM[8]. They found that the (111) surface has a higher reactivity than the (001) surface. They also investigated corrosion behavior of the (111) and (001) surfaces in 10 mM HCl solution by STM[9]. They found that the dissolution rate of the (111) surface is higher than that of the (001) surface. These results consistently show that the corrosion of the (111) surface is strongly accelerated by Cl^-.

In this experiment, the copper wires were first immersed in pure water and subsequently it was replaced with NaCl solution. Thus, before the replacement, the surface should be covered with a Cu_2O layer. The dramatic increase of the dissolution rate of the (111) surface by Cl^- suggests that the corrosion is mainly caused by the following reactions.

$$Cu_2O + 2Cl^- + 2H^+ \rightleftharpoons 2CuCl + H_2O \quad (2)$$

$$CuCl + Cl^- \rightleftharpoons CuCl_2^- \quad (3)$$

As discussed above, a Cu_2O layer formed on Cu(111) has a relatively high

crystallinity[8, 26, 34]. Thus, the dissolution should smoothly take place in a layer by layer fashion. This explains the high dissolution rate of the (111) surface in 0.1 mM NaCl solution.

A Cu_2O layer formed on Cu(110) has a higher defect density than that on Cu(111) or Cu(001). Thus, in pure water, the dissolution takes place through the defects and corrosion products made of $CuO/Cu(OH)_2$ are deposited on the surface. Kunze et al. reported that an amorphous-like layer of the corrosion products is not formed on Cu(111) but formed on Cu(001)[34]. This amorphous-like layer of the corrosion products does not serve as a good protective layer in pure water[8, 34, 37]. However, as it separates the Cu_2O surface from the solution, it should reduce the speed of reactions (2) and (3). At the same time, Cl^- may directly reacts with a copper surface through the defects. According to the previous review[5], corrosion of pure copper in Cl^- solution is caused by one of the following three reaction paths.

$$Cu + 2Cl^- \rightleftharpoons CuCl_2^- + e^- \tag{4}$$

$$Cu \rightleftharpoons Cu^+ + e^-, \quad Cu^+ + 2Cl^- \rightleftharpoons CuCl_2^- \tag{5}$$

$$Cu + Cl^- \rightleftharpoons CuCl + e^-, \quad CuCl + Cl^- \rightleftharpoons CuCl_2^- \tag{6}$$

In either case, the reaction involves transfer of Cl^- and $CuCl_2^-$ through narrow defects, which should limit the reaction rate. Thus, the overall dissolution rate of the (110) surface is not as high as that of the (111) surface in Cl^- solution.

The (001) surface has an intermediate property compared with the (111) and (110) surfaces in terms of surface energy[35], work function[36], atomic density and surface corrugation. As expected from this trend, the dissolution rate also shows an intermediate behavior. Therefore, the corrosion behavior of the (001) surface can be understood by the combination of the explanations made for the (110) and (001) surfaces. The high dissolution rate at 0.01 mM can be explained by the dissolution of both a Cu_2O layer and an underlying copper surface through the defects.

The decrease of the dissolution rate caused by the increase of Cl^- concentration from 0.01 mM to 0.1 mM can be explained by the influence of neighboring

grains. As mentioned earlier, Lapeire et al. reported that the (111) surface dissolves faster than the (001) surface when they are adjacent to each other.[7] All the (111) grains indicated by arrows 1-3 in Fig. 4 are adjacent to the (001) grains. Thus, such an influence of the neighboring grains may result in a decrease of the reaction rate on Cu(001).

5. Conclusions

In this study, nanoscale corrosion behavior of copper fine wires in dilute NaCl solution was investigated by AFM and EBSD. The major findings are summarized below.

1. The dissolution rate in pure water increases in the order of the (111), (001) and (110) surfaces due to the reactions through defects in the surface Cu_2O layer.
2. The dissolution rate of the (111) surface dramatically increases with increasing the Cl^- concentration due the dissolution of the surface Cu_2O layer as $CuCl_2^-$.
3. The dissolution rate of the (110) surface shows little dependence on Cl^- concentration probably due to the corrosion products deposited on the Cu_2O layer.

So far, investigations on the copper corrosion behavior in Cl^- solution were mostly performed at a high ionic concentration. In this study, the nanoscale corrosion behavior at a low Cl^- concentration (< 0.1 mM) was clarified. Such information should be valuable for understanding the corrosion behavior of copper fine wires in the fabrication process of semiconducting devices.

6. Acknowledgements

This work was supported by Research Grant from Hatakeyama Foundation.

References

[1] G. Hultquist, Corros. Sci. 26 (1986) 173.

[2] T. E. Eriksen, P. Ndalamba, I. Grenthe, Corros. Sci. 29 (1989) 1241.

[3] G. Hultquist, M. J. Graham, O. Kodera, S. Moisa, R. Liu, U. Bexell, J. L. Smialek, Corros. Sci. 95 (2015) 162.

[4] G. Hultquist, Corros. Sci. 93 (2015) 327.

[5] G. Kear, B. D. Barker, F. C. Walsh, Corros. Sci. 46 (2004) 109.

[6] J.-M. Song, Y.-S. Zou, C.-C. Kuo, S.-C. Lin, Corros. Sci. 74 (2013) 223.

[7] L. Lapeire, E. Martinez-Lombardia, K. Verbeken, I. D. Graeve, L. A. I. Kestens, H. Terryn, Corros. Sci. 67 (2013) 179.

[8] E. Martinez-Lombardia, Y. Gonzalez-Garcia, L. Lapeire, I. D. Graeve, K. Verbeken, L. Kestens, J. M. C. Mol, H. Terryn, Electrochimica Acta 116 (2014) 89.

[9] E. Martinez-Lombardia, V. Maurice, L. Lapeire, I. D. Graeve, K. Verbeken, L. Kestens, P. Marcus, H. Terryn, J. Phys. Chem. C 118 (2014) 25421.

[10] E. Martinez-Lombardia, L. Lapeire, V. Maurice, I. D. Graeve, K. Verbeken, L. H. Klein, L. A. I. Kestens, P. Marcus, H. Terryn, Electrochem. Comm. 41 (2014) 1.

[11] Y. Yamada, N. Konishi, J. Noguchi, T. Jimbo, J. Electrochem. Soc. 155 (2008) H485.

[12] G. Binnig, H. Rohrer, C. Gerber, E. Weibel, Phys. Rev. Lett. 49 (1982) 57.

[13] G. Binnig, C. F. Quate, C. Gerber, Phys. Rev. Lett. 56 (1986) 930.

[14] A. J. Bard, F. R. F. Fan, J. KwakK, O. Lev, Vol. 61, 1989.

[15] T. Fukuma, M. Kimura, K. Kobayashi, K. Matsushige, H. Yamada, Rev. Sci. Instrum. 76 (2005) 053704.

[16] T. Fukuma, S. P. Jarvis, Rev. Sci. Instrum. 77 (2006) 043701.

[17] T. Fukuma, Rev. Sci. Instrum. 80 (2009) 023707.

[18] K. Heinemann, D. B. Rao, D. L. Douglass, Oxid. Met. 9 (1975) 379.

[19] S. K. Chawla, B. I. Rickett, N. Sankarraman, J. H. Payer, Corros. Sci. 33 (1992) 1617.

[20] J. Itoh, T. Sasaki, T. Ohtsuka, Corros. Sci. 42 (2000) 1539.

[21] V. Maurice, H.-H. Strehblow, P. Marcus, Surf. Sci. 458 (2000) 185.

[22] H. Wieder, A. W. Canderna, J. Phys. Chem. 66 (1962) 816.

[23] T. L. Barr, J. Vac. Sci. Technol. 14 (1977) 660.

[24] N. Tajima, M. Fukui, Y. Shintani, O. Tada, J. Phys. Soc. Jap. 54 (1985) 4236.

[25] K. S. Choi, T. G. Kang, I. S. Park, J. H. Lee, K. B. Cha, IEEE T. Electron. Pack. 23 (2000) 32.

[26] J. Gao, A. Hu, M. Li, D. Mao, Appl. Surf. Sci. 255 (2009) 5943.

[27] J. W. Lim, J. Iijima, Y. F. Zhu, J. H. Yoo, G. S. Choi, K. Mimura, M. Isshiki, Thin Solid Films 516 (2009) 4040.

[28] L. Luo, Y. Kang, J. C. Yang, G. Zhou, Appl. Surf. Sci. 259 (2012) 791.

[29] L. Luo, Y. Kang, J. C. Yang, G. Zhou, Surf. Sci. 606 (2012) 1790.

[30] N. Ikemiya, T. Kubo, S. Hara, Sur. Sci. 323 (1995) 81.

[31] J. Kunze, V. Maurice, L. H. Klein, H.-H. Strehblow, P. Marcus, J. Phys. Chem. B 105 (2001) 4263.

[32] J. Kunze, V. Maurice, L. H. Klein, H.-H. Strehblow, P. Marcus, Electrochim. Acta 48 (2003) 1157.

[33] J. Kunze, V. Maurice, L. H. Klein, H.-H. Strehblow, P. Marcus, J. Electroanal. Chem. 554-555 (2003) 113.

[34] J. Kunze, V. Maurice, L. H. Klein, H.-H. Strehblow, P. Marcus, Corros. Sci. 46 (2004) 245.

[35] Y. Urano, F. Noguchi, H. Miura, J. Chem. Soc. 3 (1996) 91.

[36] P. O. Gartland, S. Berge, B. J. Slagsvold, Phys. Rev. Lett. 28 (1972) 738.

[37] Y. Feng, K.-S. Siow, W.-K. Teo, K.-L. Tan, A.-K. Hsieh, Corrosion 53 (1997) 389.

Figure 1: Schematic illustration of copper fine wires used in this study. (a) A large-scale view. (b) A magnified view of the area measured by AFM and EBSD. (c) Cross sectional view of a copper wire.

Figure 2: AFM images of copper wires in water at (a) 39 min and (b) 203 min. The 0 nm in the height scale corresponds to the approximate average height of the insulating areas. (c) IPF map of the same area as imaged by AFM. (d) Height changes at the locations indicated by the arrows No. 1 in (c).

Figure 3: AFM images of copper wires in 0.01 mM NaCl solution at (a) 68 min and (b) 177 min. The 0 nm in the height scale corresponds to the approximate average height of the insulating areas. (c) IPF map of the same area as imaged by AFM. (d) Height changes at the locations indicated by the arrows No. 1 in (c).

Figure 4: AFM images of copper wires in 0.1 mM NaCl solution at (a) 53 min and (b) 128 min. The 0 nm in the height scale corresponds to the approximate average height of the insulating areas. (c) IPF map of the same area as imaged by AFM. (d) Height changes at the locations indicated by the arrows No. 1 in (c).

Figure 5: Corrosion rates of the (110), (001) and (111) surfaces in water and 0.1/0.01 mM NaCl solution. The values correspond to an average of the values measured at the three locations indicated in Figures 2(c), 3(c) and 4(c). The only exception is the value for the (110) surface in 0.1 mM solution, where only the two (110) surface grains exist in the wire. The error bars correspond to a standard deviation of the measured values.

Figure1

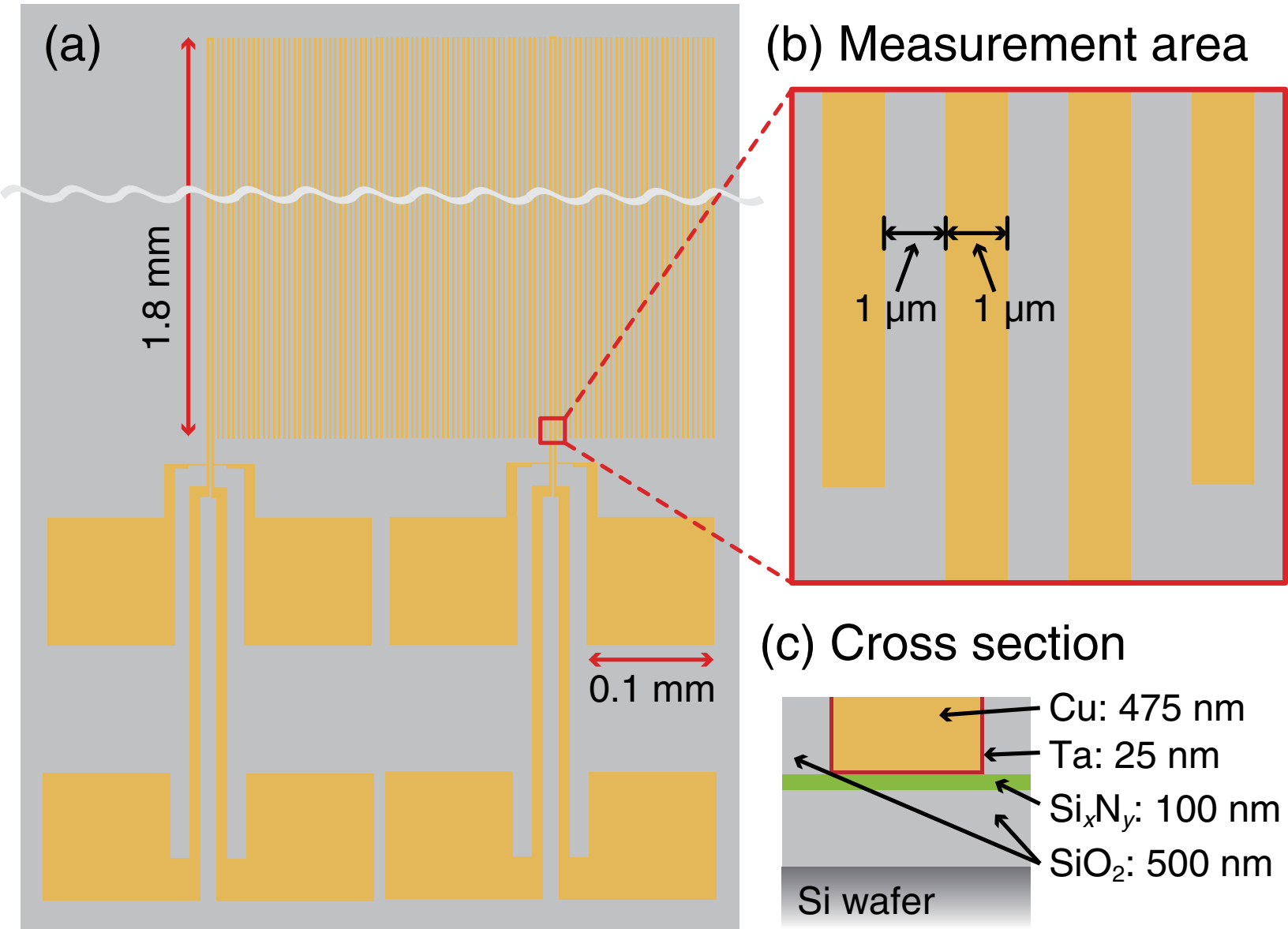
(a)
1.8 mm
0.1 mm
(b) Measurement area
1 μm
1 μm
(c) Cross section
Cu: 475 nm
Ta: 25 nm
Si_xN_y: 100 nm
SiO_2: 500 nm
Si wafer

Figure2

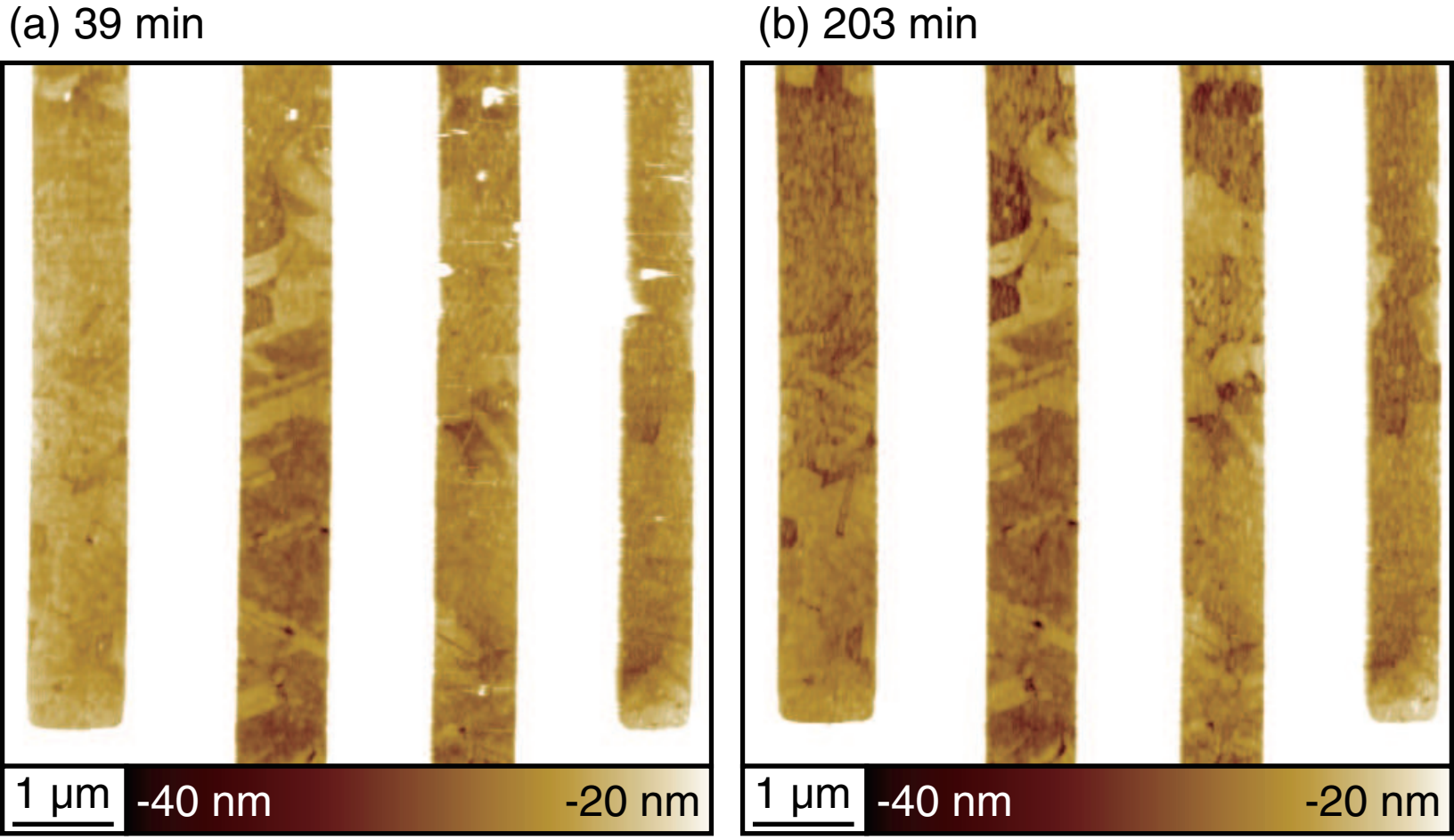
(a) 39 min
(b) 203 min
1 μm
-40 nm
-20 nm
1 μm
-40 nm
-20 nm

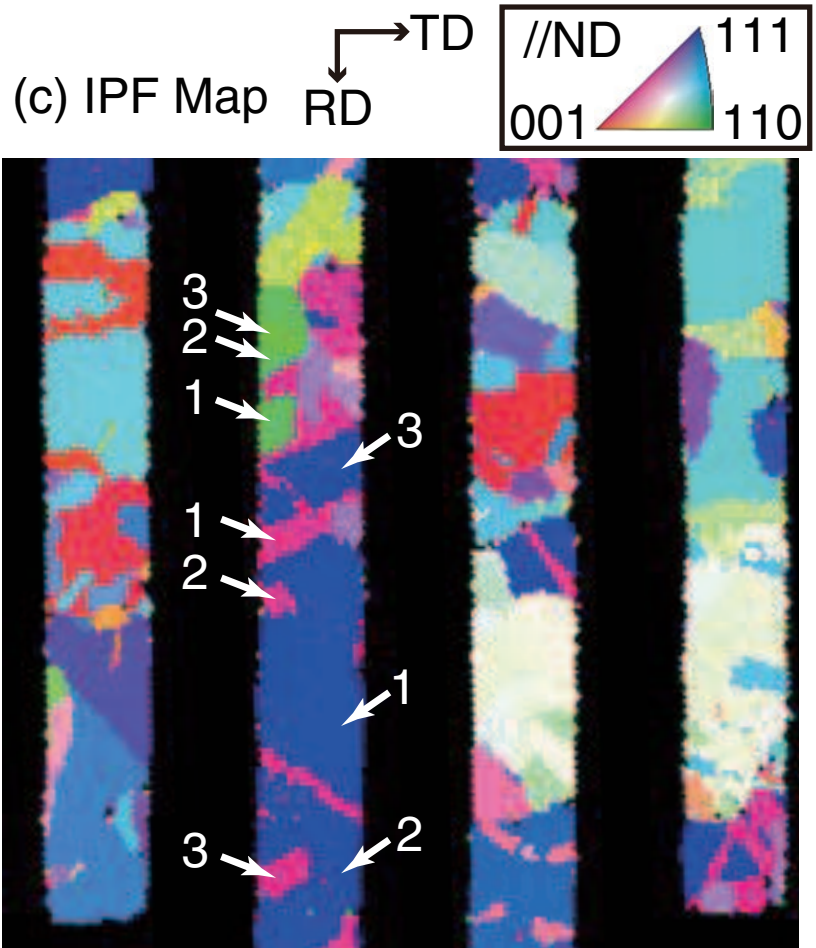
(c) IPF Map
TD
RD
//ND
111
001
110
3
2
1
3
1
2
1
3
2

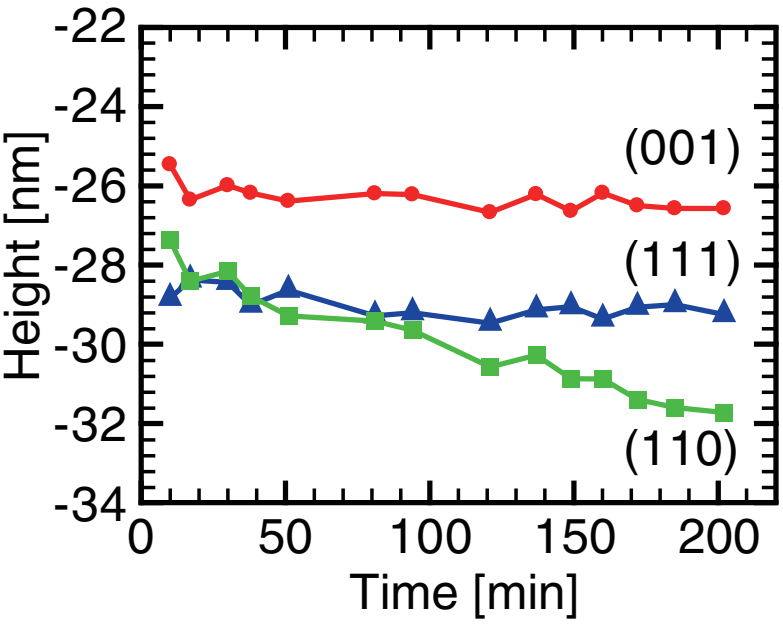
(d) Height changes at locations indicated by the arrows No. 1
Height [nm]
-22
-24
-26
-28
-30
-32
-34
0
50
100
150
200
Time [min]
(001)
(111)
(110)

Figure3

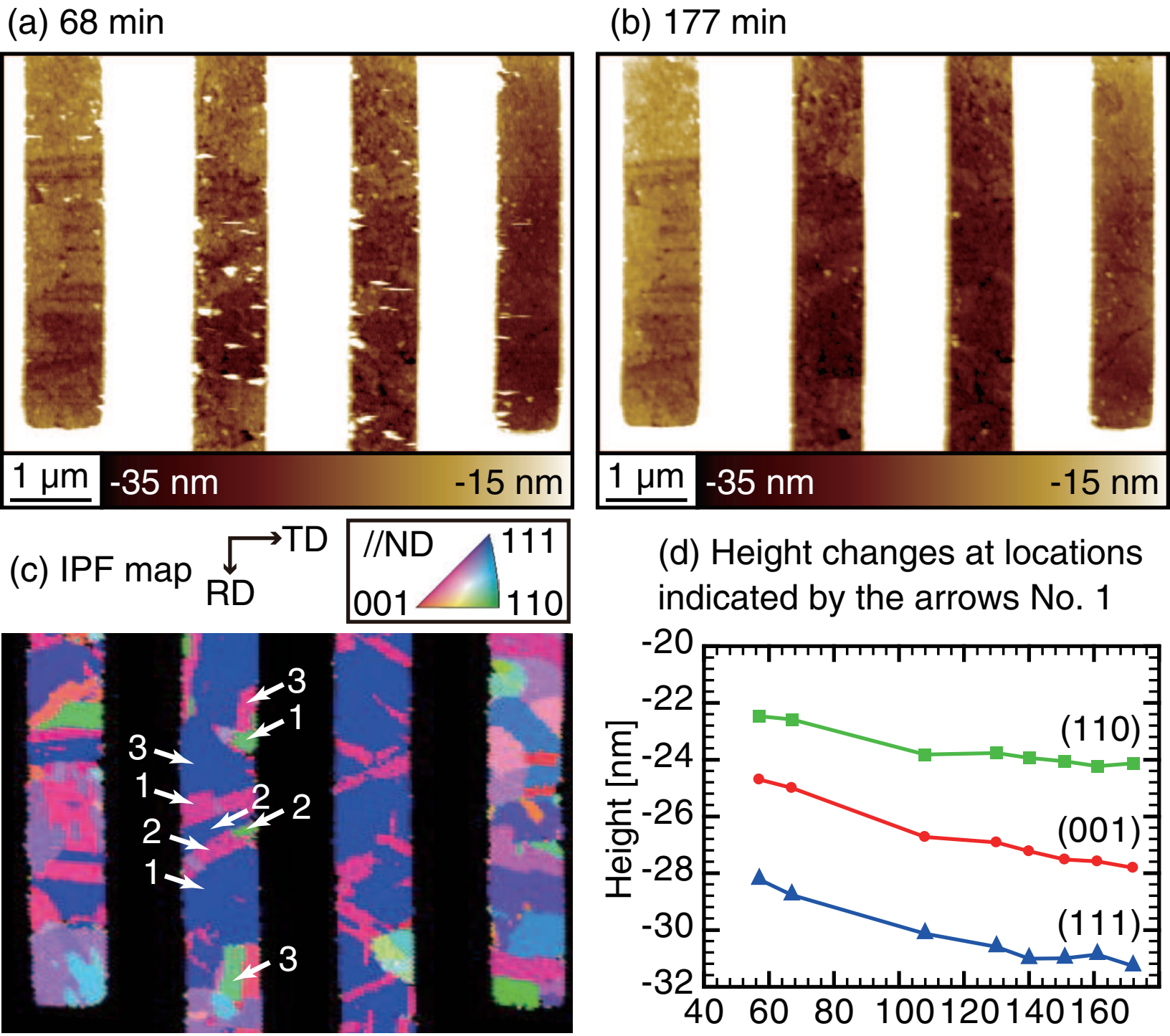
(a) 68 min
(b) 177 min
1 μm
-35 nm
-15 nm
1 μm
-35 nm
-15 nm
(c) IPF map
TD
RD
//ND
111
001
110
3
1
3
1
2
2
2
1
3
(d) Height changes at locations indicated by the arrows No. 1
Height [nm]
-20
-22
-24
-26
-28
-30
-32
(110)
(001)
(111)
40
60
80
100
120
140
160
Time [min]

Figure4

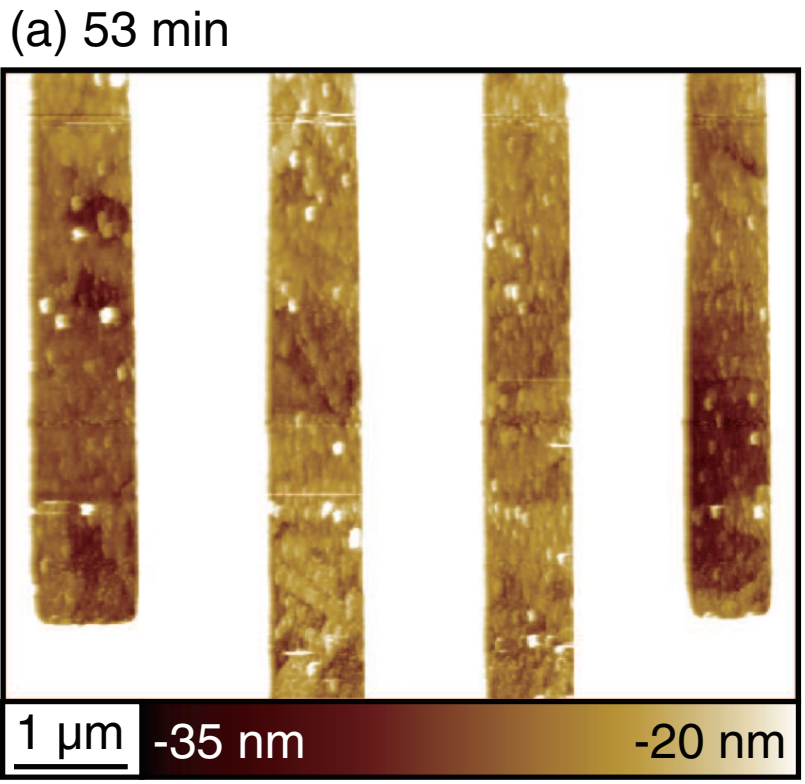
(a) 53 min
1 μm
-35 nm
-20 nm

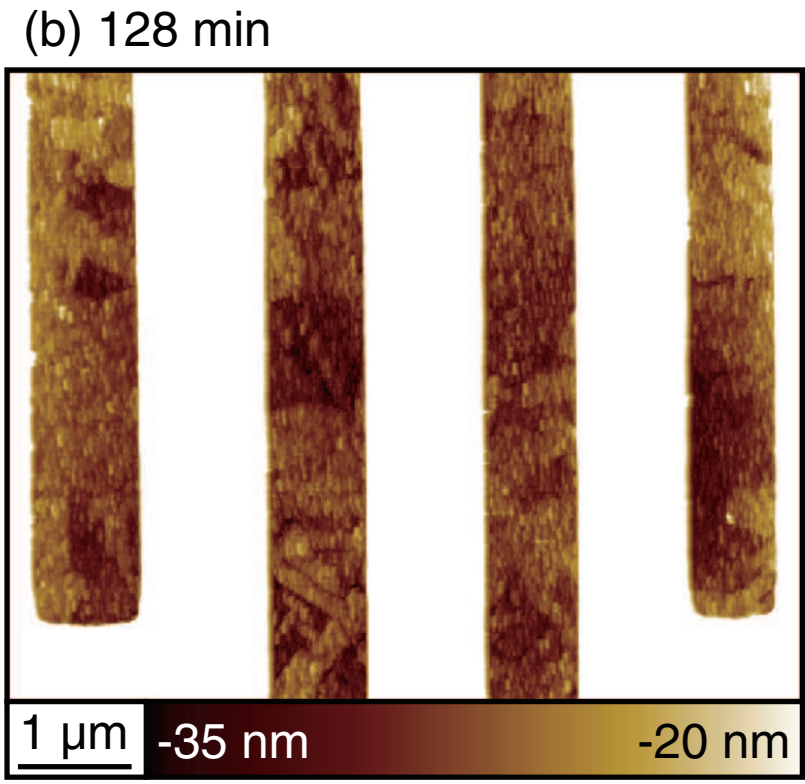
(b) 128 min
1 μm
-35 nm
-20 nm

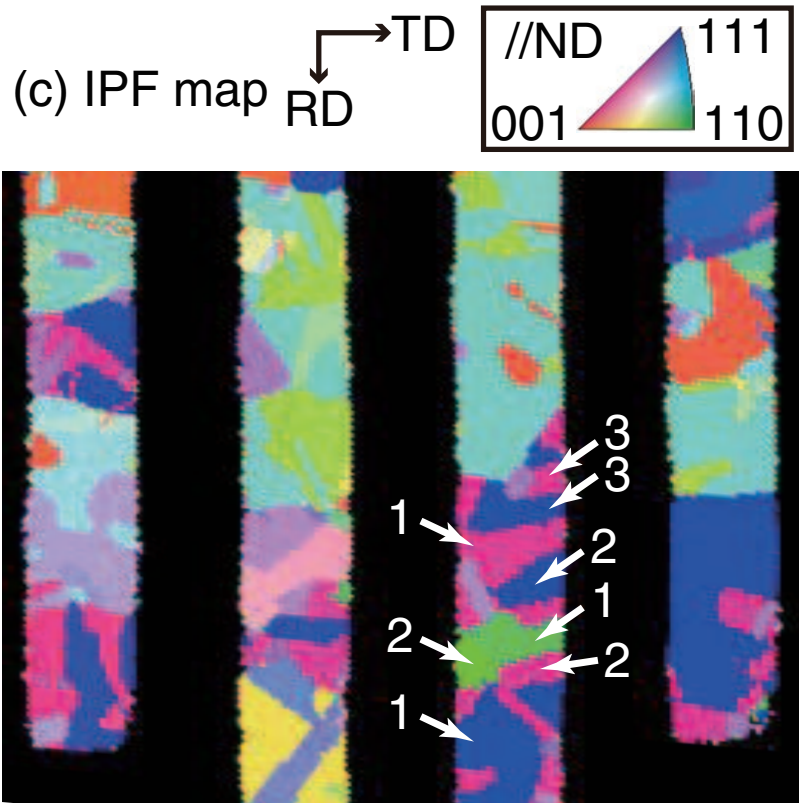
(c) IPF map
TD
RD
//ND
111
001
110
3
3
1
2
1
2
2
1

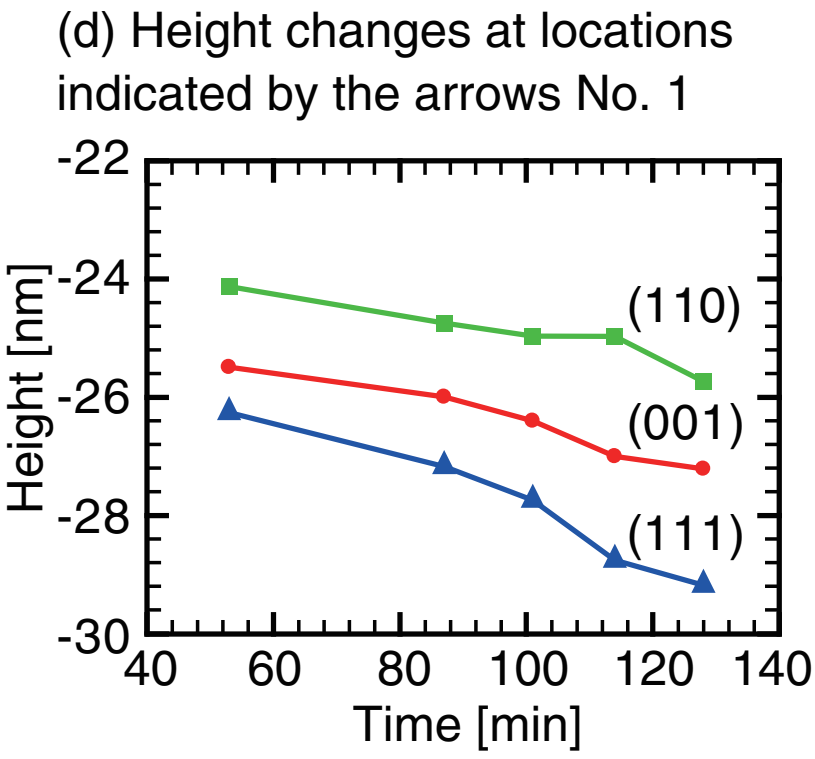
(d) Height changes at locations indicated by the arrows No. 1
Height [nm]
-22
-24
-26
-28
-30
40
60
80
100
120
140
Time [min]
(110)
(001)
(111)

Figure5

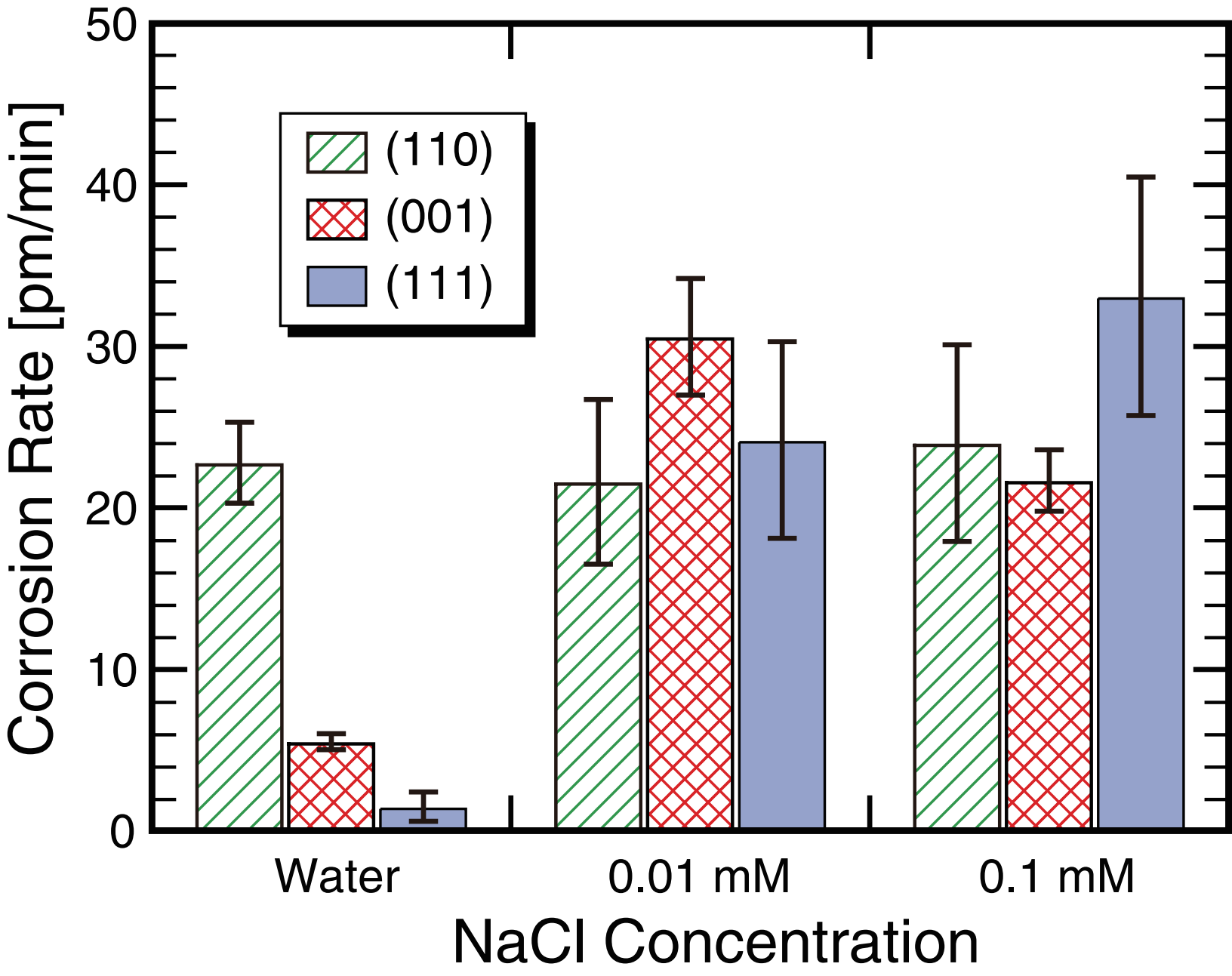
50
40
30
20
10
0
Corrosion Rate [pm/min]
(110)
(001)
(111)
Water
0.01 mM
0.1 mM
NaCl Concentration